Electronegativity explanation on the efficiency-enhancing mechanism of the hybrid inorganic–organic perovskite ABX_3 from first-principles study*

Qing-Yuan Chen(陈清源)[1], Yang Huang(黄杨)[1], Peng-Ru Huang(黄鹏儒)[1]
Tai Ma(马泰)[1], Chao Cao(曹超)[2], and Yao He(何垚)[1,†]

[1] *Department of Physics, Yunnan University, Kunming* 650091, *China*
[2] *Department of Physics, Hangzhou Normal University, Hangzhou* 310036, *China*

(Received 27 August 2015; revised manuscript received 14 October 2015; published online 20 December 2015)

Organic–inorganic hybrid perovskites play an important role in improving the efficiency of solid-state dye-sensitized solar cells. In this paper, we systematically explore the efficiency-enhancing mechanism of ABX_3 ($A = CH_3NH_3$; B = Sn, Pb; X = Cl, Br, I) and provide the best absorber among ABX_3 when the organic framework A is CH_3NH_3 by first-principles calculations. The results reveal that the valence band maximum (VBM) of the ABX_3 is mainly composed of anion X p states and that conduction band minimum (CBM) of the ABX_3 is primarily composed of cation B p states. The bandgap of the ABX_3 decreases and the absorptive capacities of different wavelengths of light expand when reducing the size of the organic framework A, changing the B atom from Pb to Sn, and changing the X atom from Cl to Br to I. Finally, based on our calculations, it is discovered that $CH_3NH_3SnI_3$ has the best optical properties and its light-adsorption range is the widest among all the ABX_3 compounds when A is CH_3NH_3. All these results indicate that the electronegativity difference between X and B plays a fundamental role in changing the energy gap and optical properties among ABX_3 compounds when A remains the same and that $CH_3NH_3SnI_3$ is a promising perovskite absorber in the high efficiency solar batteries among all the $CH_3NH_3BX_3$ compounds.

Keywords: ABX_3, efficiency-enhancing mechanism of ABX_3, optical and electronic properties, hybrid perovskite solar cells

PACS: 71.20.Rv, 78.20.–e, 78.30.Jw, 78.40.Me **DOI:** 10.1088/1674-1056/25/2/027104

1. Introduction

The hybrid inorganic–organic perovskite absorbers ABX_3 ($A = CH_3NH_3$; B = Sn, Pb; X = Cl, Br, I) have attracted lots of attention due to their outstanding performances as dye-sensitized solar-cell absorbers, topological insulators, and superconductors.[1–9] The researches of one type of the solar-cell absorber, the hybrid perovskite solar battery, have made great process in the last 5 years.[1–4] Solid-state dye-sensitized solar cells are composed of the semiconducting layer, the sensitizer, the transparent conducting and counter conducting electrodes, and the electrolyte. The working principle of solid-state dye-sensitized solar cells can be summed up as follows:

$$\text{sensitizer} + h\lambda \rightarrow \text{sensitizer}^*, \tag{1}$$

$$\text{sensitizer}^* + \text{TiO}_2 \rightarrow \text{e}^-_{\text{TiO}_2} + \text{sensitizer}^+, \tag{2}$$

$$\text{e}^-_{\text{TiO}_2} + \text{C.E.} \rightarrow \text{TiO}_2 + \text{e}^-_{(\text{C.E.})} + \text{electricalenergy}, \tag{3}$$

$$\text{sensitizer}^+ + \frac{3}{2}\text{I}^- \rightarrow \text{sensitizer} + \frac{1}{2}\text{I}_3^-, \tag{4}$$

$$\frac{1}{2}\text{I}_3^- + \text{e}^-_{(\text{C.E.})} \rightarrow \frac{3}{2}I^- + \text{C.E.} \tag{5}$$

Specifically, we can explain these equations as follows. In order to provide the surface area to adsorb sensitizers, TiO_2 is placed on the conducting electrode. When the photons irradiate on them, sensitizers are excited (Eq. (1)). The sensitizer turns into oxide when an electron is injected into the conduction band of the TiO_2. This process is described by Eq. (2). The injected electron is transported into the TiO_2 and then extracted to a load where the work done is converted into an electrical energy (Eq. (3)). The electron mediator between the TiO_2 photoelectrode and the carbon coated counter electrode is electrolytes containing I^-/I^{3-} redox ions. Hence the I^- ion redox mediator gives electrons to the oxidized sensitizer that makes the oxidized sensitizer regenerated. Then the I^- ion redox mediator turns oxide into I^{3-} (Tri-iodide ions), (Eq. (4). The I^{3-} substitutes the internally donated electron with that from the external load, reducing back to I^- ion. This process is represented by Eq. (5).[10]

The hybrid perovskite solar battery stands out due to its low cost, high efficiency, and environmental friendliness. Meanwhile, it is becoming a most promising battery compared with various solar batteries. Organic–inorganic hybrid $CH_3NH_3PbX_3$ (X = Br, I) perovskites were introduced

*Project supported by the National Natural Science Foundation of China (Grant Nos. 61366007, 11164032, and 61066005), the Program for New Century Excellent Talents in University of Ministry of Education of China (Grant No. NCET-12-1080), the Basic Applied Research Foundation of Yunnan Province, China (Grant Nos. 2011CI003 and 2013FB007), and the Excellent Young Talents in Yunnan University, China.

†Corresponding author. E-mail: yhe@ynu.edu.cn

© 2016 Chinese Physical Society and IOP Publishing Ltd

by Kojima *et al*. in 2009 as a new type of DSC sensitizing material.[11] Lee *et al*. reported a solution-processable solar cell with a conversion efficiency of 10.9%.[1] The solar conversion efficiency did not increase to 15% till recently, which was reported in a *Nature* paper by Burschka *et al*., and its high stability is equal to or even greater than those of the best thin-film photovoltaic devices.[2] As is well known, the ABX_3 absorbers with high absorption coefficients will be excellent materials for enhancing the solar-converting efficiency of the solar battery. Previously, the properties of ABX_3 were mostly investigated by several experimental studies which claimed that ABX_3 is a great solar-cell absorber due to its symmetric structure and electronic properties.[7–13] Nevertheless, theoretical researches of ABX_3 are rather rare and incomplete.[11–13]

In this study, we explore the efficiency-enhancing mechanism of ABX_3 and systematically investigate the ABX_3-type compounds which can stimulate the optical properties for hybrid inorganic–organic perovskite absorbers by first-principles calculations.[14,15] We find that the VBM and the CBM of the ABX_3 are mainly composed of anion X p states and cation B p states respectively. The band gap of the ABX_3 decreases and the absorptive capacities to different wavelengths of light expands when changing the B atom from Pb to Sn and changing the X atom from Cl to Br to I. Moreover, the organic framework A also plays an important role in ABX_3. For instance, with the size of the organic framework A increasing, the band gap increases but atoms B and X remain the same. The changing trend of the band gap will be the same when the atoms B and X change and the size of framework A remains the same. So we just examine the situation where the organic framework A remains unchanged to investigate the efficiency-enhancing mechanism of ABX_3 in this work. Finally, it is discovered that $CH_3NH_3SnI_3$ has the best optical properties, and its light-adsorption range is the widest among all the ABX_3 compounds when A remains the radical $CH_3NH_3^+$ situation based on our calculation. We also find that the electronegativity difference between X and B plays a fundamental role in changing the energy gap and optical properties among ABX_3 compounds and that $CH_3NH_3SnI_3$ is a promising perovskite absorber among $CH_3NH_3BX_3$ compounds in the high efficiency solar batteries.

2. Computational details

Our calculations were performed using the Vienna ab initio simulation package (VASP) with the projector-augmented wave (PAW) pseudopotentials.[16,17] We used the Perdew–Burke–Ernzerhof generalized gradient approximation to treat the exchange–correlation energy of interacting electrons.[18–20] The 2s, 2p electrons of C, 2s, 2p electrons of N, 1s electrons of H, 5d, 6s, 6p electrons of Pb, 2s, 2p electrons of Sn, and the 5s, 5p electrons of I were explicitly treated as valence electrons.[22,23] In order to guarantee the accuracy of the calculation, the energy cutoff for plane-wave cut-off is 500 eV. We used an A (6×6×6) Monkhorst–Pack k-point grid for geometry optimization and an A (10×10×10) grid for calculating the density of states. For the best approach to this calculation, the generalized gradient approximation (GGA) approach which is accurate and the time saving was adopted instead of the local density approximation (LDA) and HSE approach. All considered structures were fully optimized with the force on each atom being less than 0.05 eV/Å.[21,22]

ABX_3 type compound shows different phases under different temperatures. In the high temperature phase, the crystal structure of all ABX_3 adopts a cubic perovskite structure as shown in Fig. 1. It is a three-dimensional framework of a corner-sharing BX_6 octahedron in which the center is the radical group $CH_3NH_3^+$. All ABX_3-type compounds studied in this paper are based on this cubic perovskite structure.

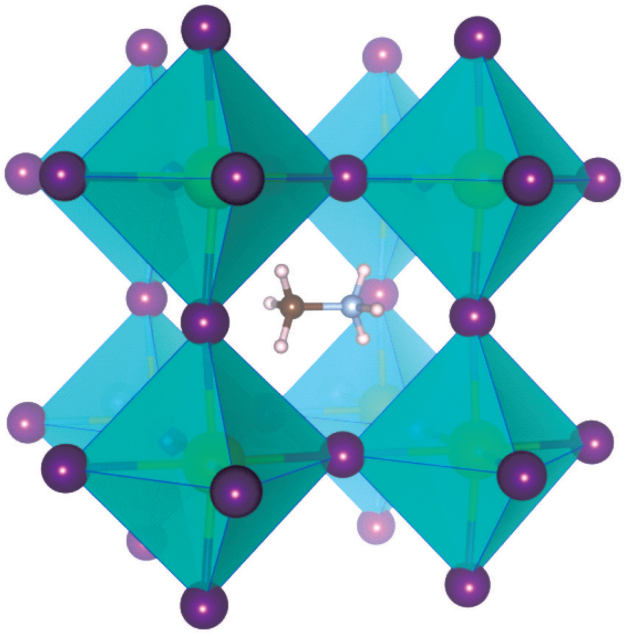


Fig. 1. (color online) Structure of ABX_3. X is shown in the vertex of the octahedron, B is shown in the center of the octabedron, the compound in the center is CH3NH3$^+$.

The computations of optical properties were carried out by the perturbation theory method that was implemented in the VASP code. The main optical spectra, such as the refractive index $N(\omega)$, reflectivity $R(\omega)$, and adsorption coefficient $I(\omega)$, all can be obtained from the dynamical dielectric response functions (ε). The explicit expressions are given by

$$\varepsilon(\omega) = \varepsilon_1(\omega) + \mathrm{i}\varepsilon_2(\omega), \tag{6}$$

$$N(\omega) = n(\omega) + \mathrm{i}k(\omega), \tag{7}$$

$$R(\omega) = \left|\frac{\sqrt{\varepsilon(\omega)-1}}{\sqrt{\varepsilon(\omega)+1}}\right|^2 = \frac{(n-1)^2+k^2}{(n+1)^2+k^2}, \tag{8}$$

$$I(\omega) = (\sqrt{2})\omega[\sqrt{\varepsilon_1(\omega)^2+\varepsilon_2(\omega)^2}-\varepsilon_1(\omega)]^{1/2}. \tag{9}$$

3. Results and discussion

3.1. Optical properties of ABX_3

ABX_3 compounds play a pivotal role in the perovskite sensitized solar cell mainly due to their optical properties which can induce the perovskite sensitized solar cells to absorb a wide range of light. According to Eqs. (1)–(5), it is clear that the wide absorptive capacities to different wavelengths of light on an absorber are the key factor in perovskite sensitized solar cells.

To find the material with the widest absorption range, the absorption coefficients of different ABX_3 compounds were calculated. We tried both the GGA approach and the LDA approach, and their results are shown in Figs. 2 and 3 respectively. Both the methods reveal the same change trend of ABX_3. Although the results from each of these two methods are not quite different from our optical calculation, the GGA method is used throughout our research because the GGA method can give a more accurate result than the experimental result through our calculating the electronic properties. As shown in Fig. 2, the absorption edge of ABX_3 moves towards the lower energy side as the X component changes from Cl to Br, and to I progressively. For compounds containing Cl, the adsorption edge is close to 3.0 eV. For compounds with I, however, the edge changes into 1.5 eV. There is about 2.0 eV reduction on the optical gap for the substitution of I for Cl. Considering compounds with different B components, the substitution of Sn for Pb also reduces the optical gap moderately. According to the results, $CH_3NH_3SnI_3$ has the smallest optical gap and thus can respond to the widest light spectra. Our calculations are consistent with experiments.[23]

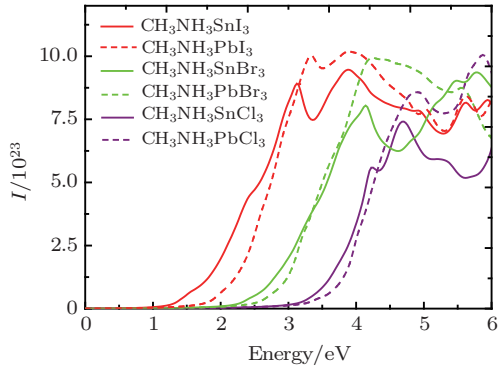


Fig. 2. (color online) Optical spectra of the absorption coefficient of ABX_3 (A = CH_3NH_3; B = Sn, Pb; X = Cl, Br, I), obtained by the GGA method.

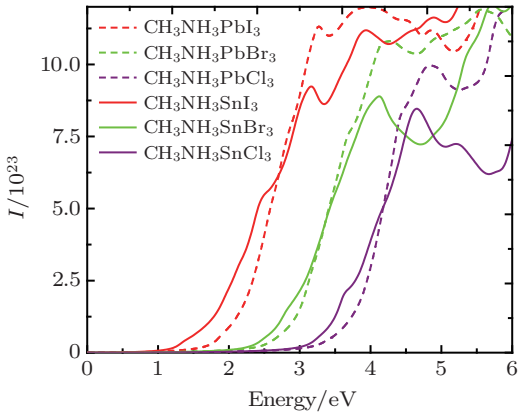


Fig. 3. (color online) Optical spectra of the absorption coefficient of ABX_3 (A = CH_3NH_3; B = Sn, Pb; X = Cl, Br, I) by the LDA method.

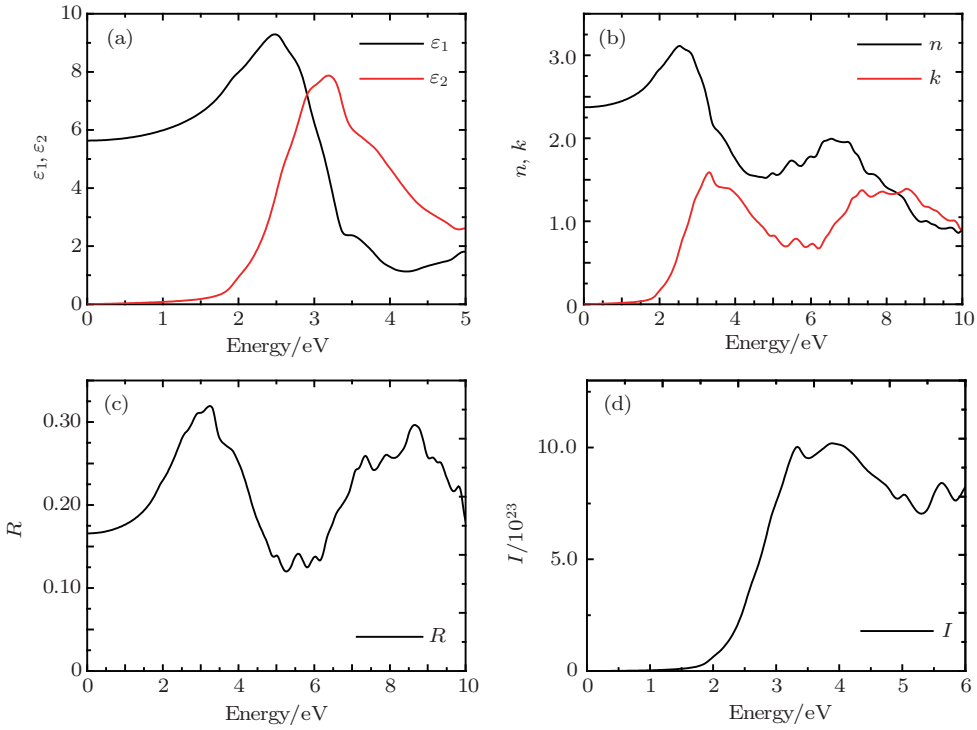


Fig. 4. (color online) Optical spectra of $CH_3NH_3SnI_3$. In panel (a), the black and red curves represent real and imaginary parts of dielectric function $\varepsilon(\omega)$, respectively. In panel (b) the black and red curves represent real and imaginary parts of refractive index, respectively. Panel (c) shows the optical spectrum of the reflectivity R. Panel (d) displays the optical spectrum of the absorption coefficient.

Figure 4 shows the detailed optical properties of $CH_3NH_3SnI_3$, obtained by DFT calculations, which is in qualitative agreement with experimental observations.[23] For zero photon frequency, the imaginary part of the dielectric function is 0 while the static dielectric constant is 6.14. The imaginary part rapidly increases with increasing the frequency in a low energy region and has a peak at 2.42 eV. This peak results mainly from the transitions of I 5p and Sn 2s states to Sn 2p states. Using Eqs. (7)–(9), the complex refractive index spectra, the reflectivity, and absorption coefficient are obtained and the results are shown in Fig. 4. The complex refractive index (Fig. 4(b)) reveals a static refraction index of 2.47. The reflectivity R is shown in Fig. 4(c). When the photon energy is in a range of 0 eV–1.34 eV and k is close to zero, R is mainly influenced by static refractive index. The first peak of R is at 2.31 eV. We can find that the $CH_3NH_3SnI_3$ has a relatively low reflectivity during ABX_3, which makes $CH_3NH_3SnI_3$ reflect less light. In Fig. 4(d), the optical spectrum of the absorption indicates comprehensive absorption information about $CH_3NH_3SnI_3$, exhibiting the correlation between the absorption and the photon energy. The photon energy 1.34 eV is the threshold that determines whether $CH_3NH_3SnI_3$ can absorb the photon energy. The optical spectrum of the absorption is caused by the radiative transitions of I 5p states and Sn 2s states to Sn 2p states. This energy belongs to all parts of visible light, thus $CH_3NH_3SnI_3$ can absorb the wavelengths of light less than 925 nm. This range of wavelengths is much wider than that of light absorbed by other ABX_3.

3.2. Electronic properties of ABX_3

To understand the trend of absorption edges of various ABX_3 compounds, their electronic properties must be addressed. According to the experimental data which we could find, the GGA method is more accurate than the LDA as shown in Fig. 5. We can see obviously that the results from the GGA method are always in better agreement with the experimental data that are shown in the blue line in Fig. 5 than those from the LDA method. In order to reduce the error of the calculation, the GGA approach, which is accurate, is adopted in our calculation.

According to the analysis of the density of states (DOS), electronic states near the band gap are governed by the orbital overlap of the BX_6 octahedron. In detail, as shown in Fig. 6, the valence band maximum (VBM) is mainly composed of B cation p states, while the conduction band minimum (CBM) is dominated by X anion p states.[24] On the other hand, the CH_3NH_3 group makes little contribution to the band edges. As a result, the energy gap of ABX_3 is determined by the cation B and anion X.[25–28]

Figure 7 shows the calculated band gaps of ABX_3 compounds with various X and B components. For compounds with the same B component, the band gap decreases monotonically as the X components change from Cl to Br and to I. This is inconsistent with the decrease in the electronegativity for each of these three elements as listed in Table 1.[29] Partial substitution of a less electronegative component for the X component also results in the decrease of the band gap. Our results accord well with the experimental data as plotted in Fig. 7. On the other hand, for compounds with the same X component, the band gap increases with the decrease in the electronegativity of the cation element. The difference between the experimental results and the calculations is mainly caused by the influence of $^3P_0$–$^3P_2$ spin–orbit splitting for Sn and Pb.

The band gaps and hence the optical edges of ABX_3 compounds are governed by the electronegativity difference between the cation B and anion X. As the VBM is dominated by anion X components and the CBM is dominated by cation B, the separation between VBM and CBM is governed by the orbital interaction of the components. From a molecular theory point of view, the orbital interaction is closely related to the relative electronegativity between cation and anion. From this consideration, the results of the band gap shown in Fig. 7 can be understood.

The electronegativity difference between cation and anion also determines the bonding nature of the BX_3 framework. As shown by the electron localization function (ELF) plotted in Fig. 8, as the X component changes from I to Br and to Cl, the bonding gets closer and closer to that of being ionic in nature. The substitution of Pb for Sn also results in a more ionic bonding.[30] For compounds studied here, $CH_3NH_3SnI_3$ is composed of components that have a most small electronegativity difference. The BX_3 framework of this compound is closest to being covalent. This compound also has a smallest band gap and can absorb the widest spectra of light.

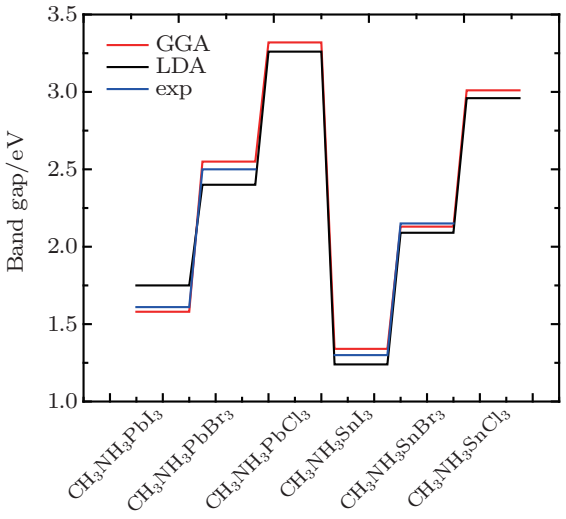


Fig. 5. (color online) Comparison of the band gaps of $CH_3NH_3BX_3$ (B = Pb,Sn; X = Cl, Br, I), obtained by the LDA method (black line), and the GGA method (red line) with experimental results (blue line).

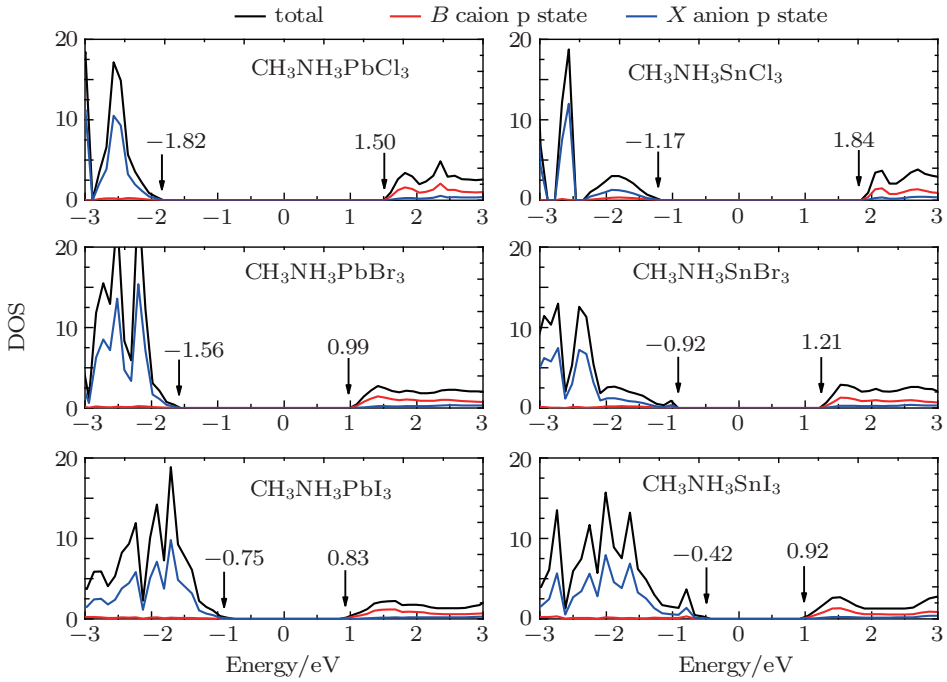


Fig. 6. (color online) Density states of $CH_3NH_3BX_3$ (B = Pb, Sn; X = Cl, Br, I).

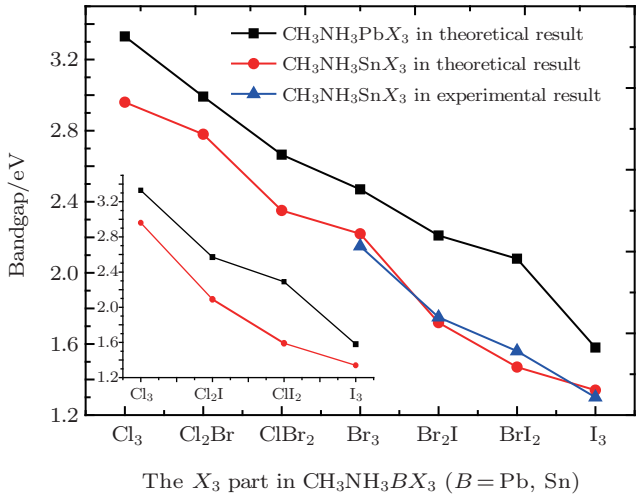


Fig. 7. (color online) Bandgaps corresponding to different matters of the ABX_3.

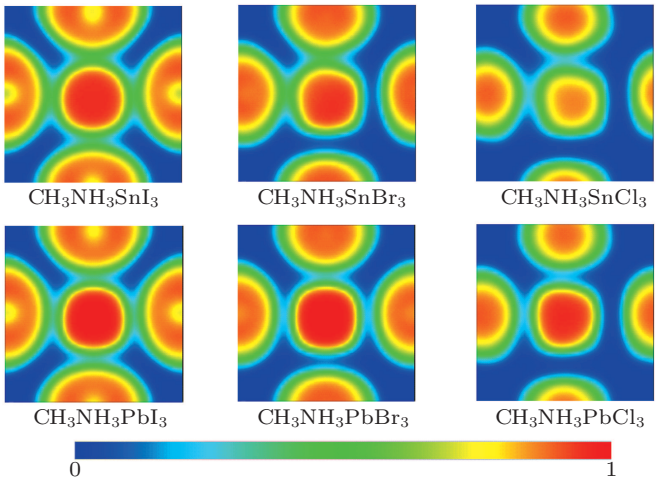


Fig. 8. (color online) ELF map of $CH_3NH_3BX_3$ compounds.

The research on the relationship between the electronegativity and the optical and electronic properties of hybrid organic–inorganic perovskites could not only reveal the change regulation of ABX_3 when the organic framework A is CH_3NH_3, but also provide a new way of explaining the basic physical efficiency-enhancing mechanism of all hybrid organic–inorganic perovskite structures ABX_3.

Table 1. Electronegativity by Pauling scale.

Element	Electronegativity
Sn	1.96
Pb	1.8
Cl	3.16
Br	2.96
I	2.66

4. Conclusions

In this work, we systematically investigate the optical and electronic properties of ABX_3 compounds through density functional calculations. For the ABX_3 compounds studied, the absorption edge has a red-shift as the anion X changes from Cl to Br and to I and the cation changes from Pb to Sn when the organic framework A remains the same. As a result, $CH_3NH_3SnI_3$ has the smallest optical gap and can respond to a very wide spectra of light. Our calculations of electronic properties of these compounds show that the fundamental band gap, consistent with the optical gap, is closely related to the cation and anion components. The variation of band gap with the component can be understood by the relative electronegativity between cation B and anion X when the

organic framework A is unchanged. Our study not only highlights the important role of $CH_3NH_3SnI_3$ for dye-sensitized solar cells, but also provides deep insight into the material engineering of ABX_3 compounds.

Acknowledgment

Computational resources are provided by High Performance Computing Center of Yunnan University.

References

[1] Lee M M, Teuscher J, Miyasaka T, Murakami T N and Snaith H J 2012 *Science* **338** 643
[2] Burschka J, Pellet N, Moon S J, Humphry-Baker R, Gao P, Nazeeruddin M K and Grätzel M 2013 *Nature* **499** 316
[3] Heo J H, Im S H, Noh J H, Mandal T N, Lim C S, Chang J A, Lee Y H, Kim H J, Sarkar A and Nazeeruddin M K 2013 *Nat. Photon.* **7** 486
[4] Stranks S D, Eperon G E, Grancini G, Menelaou C, Alcocer M J P, Leijtens T, Herz L M, Petrozza A and Snaith H J 2013 *Science* **342** 341
[5] Memming R 2001 *Semiconductor Electrochemistry*, 2nd edn. (Germany: Wiley-VCH) p. 358
[6] Kojima A, Teshima K, Shirai Y and Miyasaka T 2009 *J. Am. Chem. Soc.* **10** 1021
[7] Beiley Z M and McGehee M D 2012 *Energy Environ. Sci.* **5** 9173
[8] Jin H, Im J and Freeman A J 2012 *Phys. Rev. B* **86** 121102
[9] Takahashi Y, Obara R, Lin Z Z, Takahashi Y, Naito T, Inabe T, Ishibashi S and Terakura K 2011 *Dalton Trans.* **40** 5563
[10] Gratzel M 2005 *Chemistry* **44** 6841
[11] Kojima A, Teshima K, Shirai Y and Miyasaka T 2009 *J. Am. Chem. Soc.* **131** 6050
[12] Liu M, Johnston M B and Snaith H J 2013 *Nature* **501** 323
[13] Hodes G 2013 *Science* **342** 317
[14] Jiang Z Q, Yao G, An X Y, Fu Y J, Cao L H, Wu W D and Wang X M 2014 *Chin. Phys. B* **23** 057104
[15] Yang Z J, Liu J C, Cheng X L, Yang X D, Dai W, Li J and Guo Y D 2010 *Chin. Phys. B* **19** 077102
[16] Kresse G and Furthmuler J 1996 *Phys. Rev. B* **54** 11169
[17] Kresse G and Furthmuler J 1996 *Comput. Mater. Sci.* **6** 15
[18] Perdew J P, Burke K and Ernzerhof M 1996 *Phys. Rev. Lett.* **77** 3865
[19] Anisimov V, Zaanen J and Andersen O 1991 *Phys. Rev. B* **44** 943
[20] Tanaka T, Matsunaga K and Ikuhara Y 2003 *Phys. Rev. B* **68** 205213
[21] Brivio F, Walker A B and Walsh A 2013 *APL Materials* **1** 042111
[22] Frost J M, Butler K T, Brivio F, Hendon C H, Schilfgaarde M V and Walsh A 2014 *Nano Lett.* **10** 1021
[23] Hao F, Stoumpos C C, Cao D H and Robert 2014 *Nat. Photon.* **10** 1038
[24] Wang Y, Gould Tim, Dobson J F, Zhang H M, Yang H G, Yao X D and Zhao H J 2014 *Phys. Chem. Chem. Phys.* **16** 1424
[25] Mosconi E, Amat A, Nazeeruddin M K, Gratzel M and Angelis F D 2013 *J. Phys. Chem. C* **117** 13902
[26] Wehrenfennig C, Liu M Z, Snaith H J, Johnston M B and Herz L M 2014 *J. Phys. Chem. Lett.* **5** 1300
[27] Lang L, Yang J H, Liu H R, Xiang H J and Gong X G 2014 *Phys. Lett. A* **378** 290
[28] Brivio F, Butler K T, Walsh A and Schilfgaarde M V 2014 *Phys. Rev. B* **89** 155204
[29] Lide D R 2010 *CRC Handbook of Chemistry and Physics*, 90th edn. (The United States of America: CRC) pp. 9–77
[30] Phillps J C 1970 *Rev. Mod. Phys.* **42** 317